

Nonlinear polarization coupling in freestanding nanowire/nanotube resonators

Cite as: J. Appl. Phys. **125**, 044302 (2019); doi: [10.1063/1.5053955](https://doi.org/10.1063/1.5053955)

Submitted: 28 August 2018 · Accepted: 28 December 2018 ·

Published Online: 30 January 2019








View Online



Export Citation



CrossMark

P. Vincent,^{1,a)}  A. Descombin,¹ S. Dagher,^{1,b)}  T. Seoudi,^{1,c)}  A. Lazarus,²  O. Thomas,³  A. Ayari,¹ 
S. T. Purcell,¹ and S. Perisanu¹

AFFILIATIONS

¹Institut Lumière Matière, University of Lyon, Université Claude Bernard Lyon 1, CNRS, F-69622 Villeurbanne, France

²Sorbonne Université, CNRS, Institut Jean Le Rond d'Alembert, UMR 7190, F-75005 Paris, France

³Arts et Métiers ParisTech, LISPEN EA 7515, 8 bd. Louis XIV, 59046 Lille, France

a) pascal.vincent@univ-lyon1.fr

b) **Present address:** Univ. Grenoble Alpes, CEA, LETI, 38000 Grenoble, France.

c) **Present address:** Univ. Lyon, INSA Lyon, CNRS, LaMCoS, UMR5259, F-69621 Villeurbanne, France.

ABSTRACT

In this work, we study the nonlinear coupling between the transverse modes of nanoresonators such as nanotubes or nanowires in a singly clamped configuration. We previously showed that at high driving, this coupling could result in a transition from independent planar modes to a locked elliptical motion, with important modifications of the resonance curves. Here, we clarify the physical origins, associated with a 1:1 internal resonance, and study in depth this transition as a function of the relevant parameters. We present simple formulae that permit to predict the emergence of this transition as a function of the frequency difference between the polarizations and the nonlinear coefficients and give the “backbone curves” corresponding to the elliptical regime. We also show that the elliptical regime is associated with the emergence of a new set of solutions of which one branch is stable. Finally, we compare single and double clamped configurations and explain why the elliptical transition appears on different polarizations.

Published under license by AIP Publishing. <https://doi.org/10.1063/1.5053955>

I. INTRODUCTION

Nanotubes and nanowires (NNs) that can sustain very large mechanical oscillation amplitudes represent ideal objects for studying nonlinear effects and in particular nonlinear coupling phenomena. These nonlinearities on the one hand impose limitations for the use of NNs in applications involving nanoelectromechanical systems (NEMS), e.g., for the fundamental limit of the minimum detectable frequency shift,¹ and on the other hand, they can reveal rich and complex dynamical behaviors. Within this context, nonlinear coupling between mechanical modes in NEMS has recently become a topic of some interest.^{2–4} Such coupling can be important for NEMS applications as they can influence the resonator parameter that is being exploited. For example, one can tune the resonance frequency and quality factor of one mechanical mode through a nonlinear coupling to a second mode.^{4,5} Also, using

this coupling for a non-invasive detection means that the displacement of any mode can be detected by measuring the response of another mode.

Such couplings can be categorized in the wide family of modal interactions, known as internal resonances, that characterize coupling between several resonance frequencies that satisfy a commensurate relationship.^{6,7} References 4 and 5 correspond, for example, to (1:2) and (1:3) internal resonances phenomena. A huge amount of literature has been dedicated to internal resonances in the nonlinear dynamics community over the past 50 years, since they are commonly observed in macrostructures, for instance, in the case of nonlinear musical instruments.^{8,9} For micro/nano resonators, internal resonance received increasing attention^{10–12} over the past few years. In the special case of a resonator with two vibration modes of almost identical eigenfrequencies, a so-called one to one (1:1)

internal resonance can be observed. This occurs especially in the case of resonators with particular symmetries, such as circular or square plates, for which the coupling is observed between degenerate companion modes.^{13,14} The same property occurs for beams with a symmetrical cross section, between the degenerate modes in the two transverse orthogonal directions or polarizations. Among others, see Ref. 15 in the case of a string, Refs. 16 and 17 in the case of clamped-clamped beams, and Refs. 18 and 19 for a singly clamped beam.

In the case of NEMS, we previously showed experimentally, for a singly clamped configuration,²⁰ that beyond the classical Duffing phenomenon characterized by jumps and hysteresis, a transition from planar to elliptic vibration occurs for the higher frequency polarization. Simulations of the dynamics using a model based on cubic nonlinear coupling terms between the polarizations were in good agreement with the experiments. This succinct treatment opens many interesting questions of direct interest for experiments such as the dependence of the threshold of the elliptical transition on vibration amplitude and the frequency difference between polarizations, whether the transition can appear on the first polarization, etc. Here, we go beyond the original basic dynamical simulations with a self consistent approach (see next) and also develop semi-analytic and predictive formulae allowing an in-depth understanding of this rich phenomenon.

The numerical simulations have been realized using the MANLAB²¹ software which is a free Matlab package that combines the harmonic balance method (HBM) and a continuation method²² to follow the periodic solutions of dynamical system when a control parameter is varied. Moreover, it includes stability analysis based on computing the Floquet exponents in the frequency domain with a Hill eigenvalue problem.^{23,24} The analytical treatment is used to clarify the physical origins of this transition and gives simple formulae for the transition depending on the geometric parameters of the NNs. The validity of these formulae is confirmed by comparison with simulations. Finally, simulations were also used to explore more widely the phase space of these equations, allowing us to present a new set of solutions that appears as a consequence of the elliptical transition.

II. EXPERIMENTAL OBSERVATION

It is useful to start by giving a brief description of the experimental observations. The transition was first observed during field emission (FE) experiments on nanowires²⁰ in which an applied voltage causes electrons to be emitted from the nanowire apex. They are then accelerated by the field onto a viewing screen placed at several centimeters which gives a projection image of the apex emission zone. The nanowires were electrostatically excited during FE and the cycle-averaged variation of the FE pattern serves for motion detection. The FE configuration has the advantage of giving a greatly magnified image ($\sim 10^5$) of the apex displacement in the x-y plane²⁵ so that the elliptical transition is a clear and even striking phenomenon. Direct observations of the oscillations²⁰ and the elliptic transition of various excited NNs were also

carried out in both Scanning and Transmission Electron Microscopes (SEM and TEM) that confirmed the FE experiments. Experiments have been carried out extensively on SiC nanowires having resonant frequencies for the fundamental mode between a few kilohertz and a few megahertz depending on their dimensions. Their pristine quality factors range from a few hundred to several tens of thousands in vacuum. A rapid heat treatment is generally realized and quality factors between few tens of thousands and up to 100 000 can be obtained.²⁶

Figure 1 shows SEM observations of the elliptical movement of a SiC nanowire stuck at the end of a large tungsten support tip. The NN is excited by an open loop piezoelectric actuation. The sample is positioned so that the nanowire points almost along the electron beam axis, giving a very shortened projection in the image plane [Fig. 1(a), NN at rest]. Though this configuration is a little tricky to visualize, the advantage is that the images follow quite directly the movement in the x-y plane (perpendicular to the length of the wire) of the NN apex (for more details, see Fig. 1 of the [supplementary material](#)). As the excitation frequency is increased, the lower planar polarization is first observed [Fig. 1(b)] resulting in a straight line in the image. At higher frequency the second planar polarization is observed orthogonal to the first

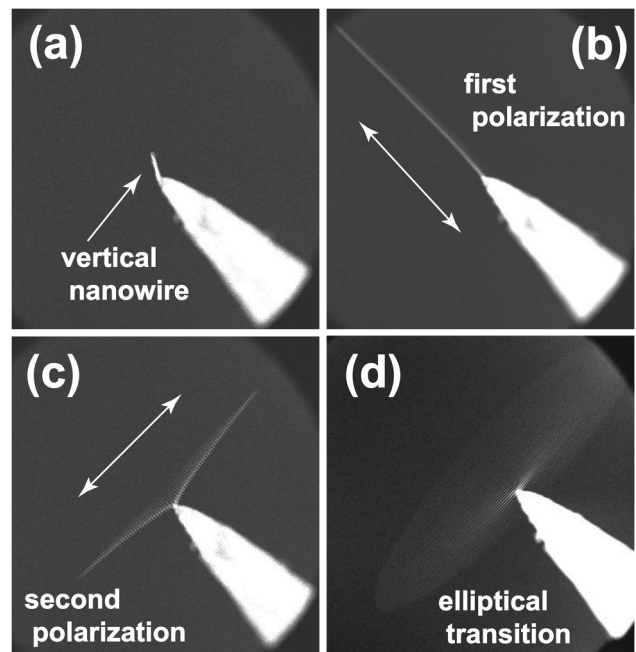


FIG. 1. SEM images of a resonating nanowire and the apparition of the transition characterized by elliptical oscillations. (a) The nanowire at rest. The nanowire is almost vertical and the projected length is very small. (b) and (c) The two orthogonal and planar polarizations corresponding to the fundamental mechanical mode. (d) Beyond the transition, we observe the elliptical oscillations.

polarization [Fig. 1(c)] which increases in amplitude as the resonance is swept (the somewhat non-linear shape is due to the rather convoluted projection of a tilted, oscillating, finite-length nanowire). At a certain amplitude (or frequency), the planar oscillation starts to become elliptical. As the frequency is increased above this transition, the size of the ellipse slowly increases and its eccentricity decreases [Fig. 1(d)]. The NN resonance ends with a jump to zero amplitude like a classic hard spring Duffing behavior.

III. ANALYTICAL MODEL

We demonstrated previously that cubic coupling terms were sufficient to explain this elliptical transition. This two dimensional model can be written in the following form (see Refs. 20 and 19 and the [supplementary material](#) for detailed treatment):

$$\begin{aligned} [1 + \beta(x^2 + y^2)]\ddot{x} + \frac{1}{Q}\dot{x} + [1 + \alpha(x^2 + y^2) + \beta(\dot{x}^2 + \dot{y}^2)]x \\ = F_1 \cos(\Omega t), \end{aligned} \quad (1)$$

$$\begin{aligned} [1 + \beta(x^2 + y^2)]\ddot{y} + \frac{1}{Q}\dot{y} + [1 + 2\mu + \alpha(x^2 + y^2) + \beta(\dot{x}^2 + \dot{y}^2)]y \\ = F_2 \cos(\Omega t), \end{aligned} \quad (2)$$

where x and y correspond to the two dimensionless orthogonal polarization directions and the displacements of the free apex normalized to the total length of the wire. The coefficients α and β are coupling terms that depend on the mode considered (see the [supplementary material](#)). Practically, they

correspond to the nonlinear terms in potential and kinetic energy, respectively. Q is the quality factor of the resonance (assumed equal for both polarizations) and μ represents the frequency difference between the two polarizations. Ω is the external excitation frequency, and we use two different excitations F_1 and F_2 as experimentally the excitations are never exactly symmetric. Note that, in the following, we will always consider the case where the two polarizations are well separated. Formally, these conditions can be written $\mu > 2/Q$, that is our case experimentally.

To emphasize the consequences of the coupling between the polarizations, simulations presented in Fig. 2 are realized with and without the coupling between the polarizations using Eqs. (1) and (2) implemented in MANLAB. In the second case, the nonlinear terms are preserved but without the crossed coupling between the polarizations as presented in Ref. 27 or in the [supplementary material](#). The frequency difference between the polarizations is 0.5% and the intrinsic quality factor of each mode is $Q = 5000$. Excitations (F_1, F_2) are chosen to obtain a maximum normalized amplitude of 0.1 and 0.2, respectively, for the x and y polarizations ($QF_1 = 0.1$ and $QF_2 = 0.2$). The values of α and β correspond to tabulated values for the fundamental mode shape (see the [supplementary material](#)). Simulation results then give the different harmonic components of $x(t)$ and $y(t)$ at $\Omega, 2\Omega, 3\Omega\dots$ The first harmonic response of $x(t)$ and $y(t)$, plotted in Fig. 2, can then be written in the form $x(t) = R_x \cos(\Omega t + \theta)$ and $y(t) = R_y \cos(\Omega t + \theta + \varphi)$. R_x and θ (respectively, R_y and $\theta + \varphi$) are plotted in blue (resp. red) and the relative phase, φ , is plotted in black in (b) and (d).

For the uncoupled equations [Figs. 2(a) and 2(b)], the two classical planar resonances with hard-spring behavior are observed (stable solutions are drawn using thick lines, whereas unstable solutions are presented with thin lines). Simulations using exactly the same parameters than in (a) and (b) but with the coupling terms between the polarizations are presented in (c) and (d). For the lower polarization, no important modification is observed. The situation changes radically for the second polarization. For low amplitudes, we still observe planar oscillations. However, above a critical amplitude, we observe a strong modification of the amplitude-frequency curve of the y polarization and the x polarization is once again excited. In the phase figure, this transition is characterized by a phase difference φ that locks on the value $\pi/2$. This leads to an elliptical movement in which the major axis corresponds to y and the minor axis to x , as experimentally observed. As the frequency is increased, the phase difference φ is fixed, while θ still varies and the eccentricity of the ellipse decreases (the ellipse tends toward a circle). After the transition, the range of frequencies for which the elliptical oscillations continue is very large and the jump corresponds to a lower y amplitude compared to the uncoupled case. Note that the fact that no transition occurred on the x polarization does not depend of the chosen parameters. As we will see later, it is a generic effect that is the result of the nonlinearities of the problem.

To go further in the analysis, it is convenient to seek the solutions in the form $x(t) = R_x \cos(\Omega t + \theta)$ and $y(t) = R_y \cos(\Omega t + \theta + \varphi)$. Injecting these forms and neglecting the higher

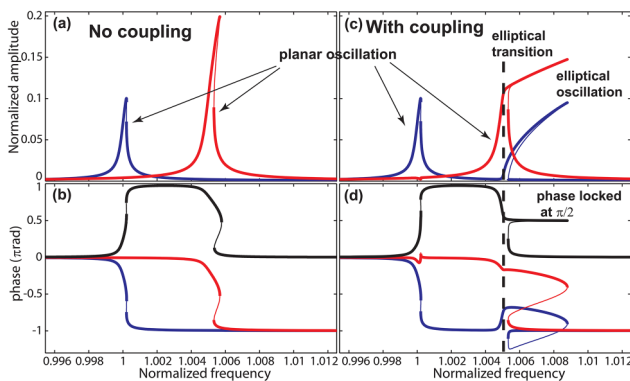


FIG. 2. Simulated resonance curves for the amplitude and phase of the two polarizations of the fundamental mode without [(a) and (b)] and with [(c) and (d)] the nonlinear coupling terms between polarizations (more precisely, the curves (c) and (d) were obtained from Eqs. (1) and (2), whereas (a) and (b) were obtained from equations presented in Ref. 27). Responses of the x and y polarizations are presented, respectively, in blue and red. Stable and unstable solutions are presented with thick lines and thin lines, respectively. Without coupling, only classical hard spring Duffing behavior is observed. With coupling, the emergence of the elliptical oscillations is observed on the higher frequency polarization.

order terms (see the [supplementary material](#) for two time scale treatment), the following equations are obtained, after some algebraic manipulation:

$$\ddot{x} + \left[\frac{1}{Q} + \frac{R_y^2}{4} \sin(2\varphi)(\alpha - 2\beta) \right] \dot{x} + \left\{ 1 + \frac{R_x^2}{4}(3\alpha - 2\beta) + \frac{R_y^2}{4}[2\alpha + \cos(2\varphi)(\alpha - 2\beta)] \right\} x = F_1 \cos(\Omega t), \quad (3)$$

$$\ddot{y} + \left[\frac{1}{Q} - \frac{R_x^2}{4} \sin(2\varphi)(\alpha - 2\beta) \right] \dot{y} + \left\{ 1 + 2\mu + \frac{R_x^2}{4}(3\alpha - 2\beta) + \frac{R_y^2}{4}[2\alpha + \cos(2\varphi)(\alpha - 2\beta)] \right\} y = F_2 \cos(\Omega t). \quad (4)$$

One can immediately identify the prefactors of x , \dot{x} , y , and \dot{y} with effective frequencies and dissipations and see that they are interdependent through the amplitudes and phases of the transverse oscillations. To simplify further, first define the effective x and y quality factors as

$$\frac{1}{Q_{x,\text{eff}}} = \frac{1}{Q} + \frac{\alpha - 2\beta}{4} R_y^2 \sin 2\varphi, \quad (5)$$

$$\frac{1}{Q_{y,\text{eff}}} = \frac{1}{Q} + \frac{\alpha - 2\beta}{4} R_x^2 \sin 2\varphi \quad (6)$$

and effective x and y frequencies as

$$\omega_{x,\text{eff}}^2 = 1 + \frac{R_x^2}{4}(3\alpha - 2\beta) + \frac{R_y^2}{4}[2\alpha + \cos(2\varphi)(\alpha - 2\beta)], \quad (7)$$

$$\omega_{y,\text{eff}}^2 = 1 + 2\mu + \frac{R_x^2}{4}(3\alpha - 2\beta) + \frac{R_y^2}{4}[2\alpha + \cos(2\varphi)(\alpha - 2\beta)]. \quad (8)$$

The equations then become

$$\ddot{x} + \frac{\dot{x}}{Q_{x,\text{eff}}} + \omega_{x,\text{eff}}^2 x = F_1 \cos(\Omega t), \quad (9)$$

$$\ddot{y} + \frac{\dot{y}}{Q_{y,\text{eff}}} + \omega_{y,\text{eff}}^2 y = F_2 \cos(\Omega t). \quad (10)$$

Particularly, Eqs. (7) and (8), which define the effective frequencies as a function of the amplitude of the system response when neither damping nor forcing are present, are called the “backbone curves” of the x and y polarizations. These backbone curves will be used intensively for analytical treatments. One of the most important aspects is that the frequency of one polarization is tuned by the other polarization. This tuning depends on the square of the amplitude of the other polarization and on the relative phase, φ . In fact, for the fundamental mode shape, we have $2\alpha = 1.6356$ and $\alpha - 2\beta = -1.48$

so that the coupling always leads to an increase of the effective frequency of the other polarization. In Eqs. (5) and (6), the evolution of the quality factors reveals the internal energy exchange between polarizations as discussed in more detail in the [supplementary material](#).

One can notice that the analytical approach followed in the present article to derive analytical solutions, based on ansatz functions for $x(t)$ and $y(t)$, is pragmatic and is, as it will be shown, validated by numerical simulations. A more mathematically rigorous analysis would have been to apply a perturbation method (such as the multiple scale method⁶) that would have given additional results about the stability of the solution branches and the type of bifurcations. This kind of analysis has been proposed for 1:1 internal resonance in mechanical structures in moderate rotations, based on Eqs. (1) and (2) with $\beta = 0$, in Ref. 28 for the free response and in Ref. 29 for the forced response. The extension of those analysis for the case $\beta \neq 0$ is not available in the literature at the moment and is left for further studies.

IV. RESULTS

Now let us examine the emergence of the elliptical transition only on the second polarization. As mentioned in Fig. 1, an important aspect used for our analytical treatment is that near the transition, φ is very close to $\frac{\pi}{2}$. When the second polarization is excited, the increase of R_y increases the effective frequency of the x polarization. If this frequency increases until it reaches the excitation frequency, the x polarization will be once again excited. This is the key to understand the elliptical transition. To determine the conditions in which this transition can occur, let us examine the evolution of these frequencies. As $\varphi \sim \frac{\pi}{2}$, we can write the effective frequency of the x polarization as (before the transition, R_x is negligible)

$$\omega_{x,\text{eff}} = 1 + R_y^2(\alpha + 2\beta)/8. \quad (11)$$

In the same conditions, the backbone curve of the y polarization is given by

$$\Omega = 1 + \mu + R_y^2(3\alpha - 2\beta)/8. \quad (12)$$

If we consider that the transition occurs when $\omega_{x,\text{eff}} = \Omega$ (that is a slight overestimation as we will see later), we obtain the critical amplitude $R_{y,c}$ for which the transition occurs and that is given by

$$R_{y,c} = \sqrt{\frac{4\mu}{-\alpha + 2\beta}}. \quad (13)$$

The critical amplitude simply depends on the frequency difference between the polarizations and the nonlinear coupling terms. Now, during the elliptical movement, the effective resonance frequencies of the x and y polarizations are nearly the same. Equalizing the two (taking $\varphi \sim \frac{\pi}{2}$) gives the relation

between R_x and R_y and we obtain $R_x^2 \simeq R_y^2 - R_{y,c}^2$. Re-injecting this relation into Eqs. (7) and (8), one obtains the backbone curves for R_x and R_y versus the frequency throughout the elliptical regime (denoted $\omega_{y,e}$ and $\omega_{x,e}$ with e for elliptical). Practically, we obtain

$$\omega_{y,e} = 1 - \frac{\mu}{2} \left(\frac{3\alpha - 2\beta}{-\alpha + 2\beta} \right) + \frac{\alpha}{2} R_y^2, \quad (14)$$

$$\omega_{x,e} = 1 + \frac{\mu}{2} \left(\frac{\alpha + 2\beta}{-\alpha + 2\beta} \right) + \frac{\alpha}{2} R_x^2. \quad (15)$$

Note that, for the fundamental mode shape, we have $\frac{3\alpha - 2\beta}{-\alpha + 2\beta} = 0.104$ and $\frac{\alpha + 2\beta}{-\alpha + 2\beta} = 2.1$. Practically, the backbone curve for the y polarization is little sensitive to μ and we can reasonably write $\omega_{y,e} \simeq 1 + \frac{\alpha}{2} R_y^2$.

MANLAB simulations using various frequency differences that demonstrate the validity of our analytical formulae are presented in Fig. 3. For simplicity, the natural frequency of the x polarization is set to 1 and the frequency difference is modified by varying the value of μ . Simulations with frequency differences of 0.5%, 1%, 2%, 2.5%, and 3% and an excitation F_2 that corresponds to a normalized maximum amplitude of 0.25 in the y direction are given. The backbone curves for the y and x polarizations during the transition [Eqs. (14) and (15)] are plotted using the black dotted lines for $\mu = 0.5\%$. There is a good quantitative agreement between our analytical formulae and simulations. For 0.5%, 1%, and 2%, the amplitude R_y reaches the critical amplitude and the elliptical transition occurs. The limit case corresponds to $\mu = 2.5\%$. For a higher μ (and for our chosen excitation), no transition occurs, and we only observe the classical case as if the polarizations were uncoupled. Of course, it does not mean that no elliptical transition could appear for a frequency difference of 3%, but it would require higher excitation.

To clarify this aspect, the inset of Fig. 3(b) presents the normalized critical amplitude $R_{y,c}$ versus the frequency difference between polarizations following Eq. (13). According to the graph, the elliptical transition should easily be observed for μ of a few percent that can be obtained for a large variety of nanowires or nanotubes. If a maximum normalized amplitude of 0.4 is considered, which can in practice be obtained for the fundamental mode, the elliptical transition should be observed for all nanowires with $\mu < 5\%$. In fact, it is surprising that such behavior is not more often reported in the literature. Note that for superior modes, the elliptical transition appears for much lower amplitudes as we will see later.

We have seen that the transition occurred when the higher polarization hardened the lower polarization enough so that it could once again be excited by the driving frequency. For the fundamental mode, this is the only possibility as the parameters show that the excitation of one polarization can only increase the frequency of the other. To better visualize this effect, we present in Fig. 4 the effective frequencies $\omega_{x,eff}$ and $\omega_{y,eff}$ of the two polarizations as a function of the excitation frequency. This is done by taking the oscillation

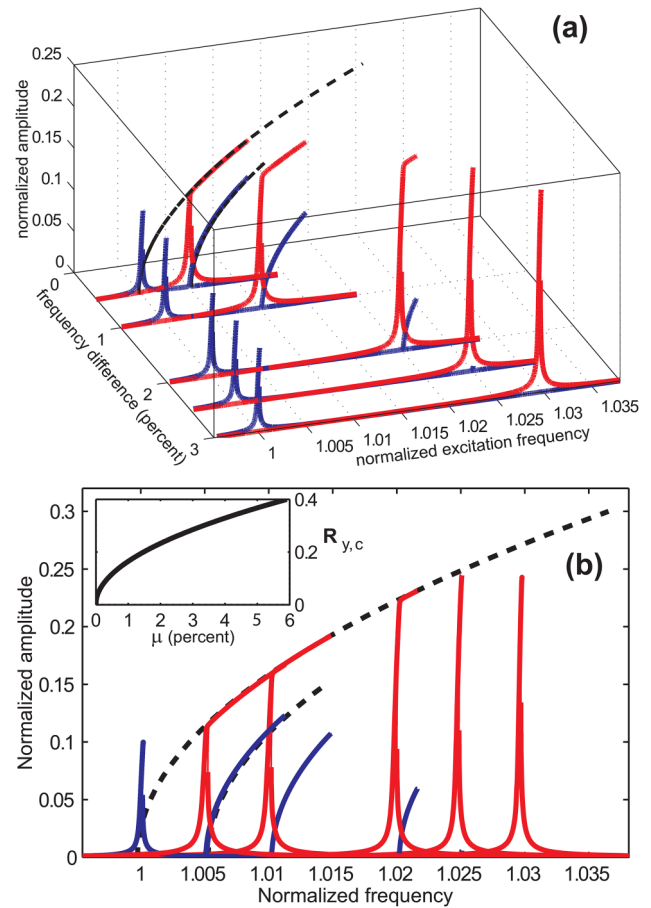


FIG. 3. Simulations showing the evolution of the elliptical transition as a function of the frequency difference between the polarizations. The simulations correspond to frequency differences of 0.5%, 1%, 2%, 2.5%, and 3%. The black dashed lines trace the backbone curves corresponding to the elliptical regime for $\mu = 0.5\%$ following Eqs. (14) and (15). (a) 3 dimensional representation of the different response curves. (b) Projection of the response curves showing that the different transitions are well fitted by the backbone curve. Inset: Evolution of the critical amplitude, $R_{y,c}$, versus the frequency difference, μ .

parameters from MANLAB simulations and re-injecting them into the frequency dependance in Eqs. (7) and (8). The blue line represents the lower (x) effective frequency $\omega_{x,eff}$, the red line the higher effective frequency $\omega_{y,eff}$, and the black line the excitation frequency. As expected, when the lower polarization is excited, it increases the effective frequency of the other polarization and no transition can occur. In contrast when the second polarization is excited, the lower effective frequency is pulled toward the excitation frequency and the x polarization is once again excited. Once the elliptical transition is activated, the nonlinear terms couple the two polarizations together and they start to behave as a strong hard spring resonator that can be excited over a large frequency range. We can also observe that even if the $\omega_{x,eff}$ is increased almost

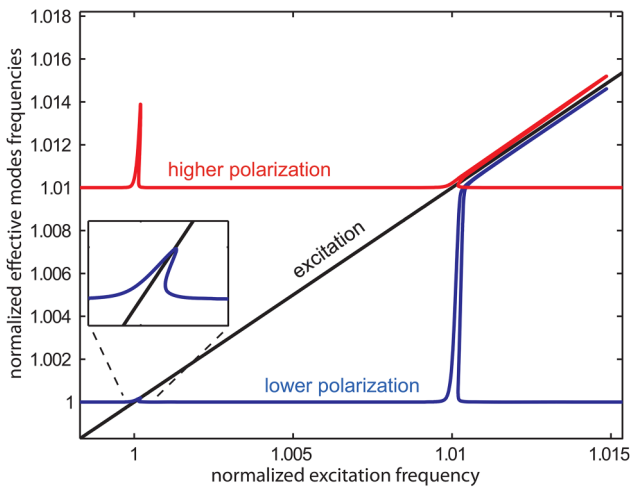


FIG. 4. Evolution of the effective frequencies of the polarizations as a function of the excitation frequency. When the first polarization is excited, the frequency of the higher polarization is further increased and no transition is possible for the lower polarization. As the second polarization is excited, the effective frequency of the lower polarization is increased almost at the frequency of the higher mode and the elliptical oscillations begin.

to the excitation frequency, it remains, however, always slightly inferior. This explains that in our analytic treatment where we defined the beginning of the transition for $\omega_{x,eff} = \Omega$, we made a small overestimation. However, the fact that our formulae fit correctly the simulations confirms that our approximation is reasonable.

An interesting question is whether the elliptical solutions presented above are the only solutions in the presence of the nonlinear coupling. In fact, we show next that the elliptical regime leads to the emergence of another independent set of solutions. Figures 5(a) and 5(b) present amplitude and phase diagrams of these new solutions obtained by MANLAB. Depending on the excitation frequency, we can have zero, two, or four solutions. More importantly, the stability analysis predicts that one part of these solutions is stable and hence physically obtainable. To better understand these new solutions, Fig. 5(c) shows the superposition of all the solutions and it can be seen that the closed curve of the new solutions corresponds partially to the truncated part of the classical Duffing mode of an independent y resonance. One can distinguish two branches in this new set of solutions. One branch corresponds to the higher part of the planar excitation of the y polarization. However, this part is now unstable. The second branch corresponds to another elliptical oscillation and one part of these solutions is stable. As before, we see in the phase diagram that the relative phase between the polarizations for the new elliptical solutions is locked but this time at the value $\varphi = -\pi/2$. The inset in Fig. 5(c) presents a zoom of the solutions in the elliptical zone. We see that the two stable elliptical solutions become very close in amplitude, the new elliptical solution, however,

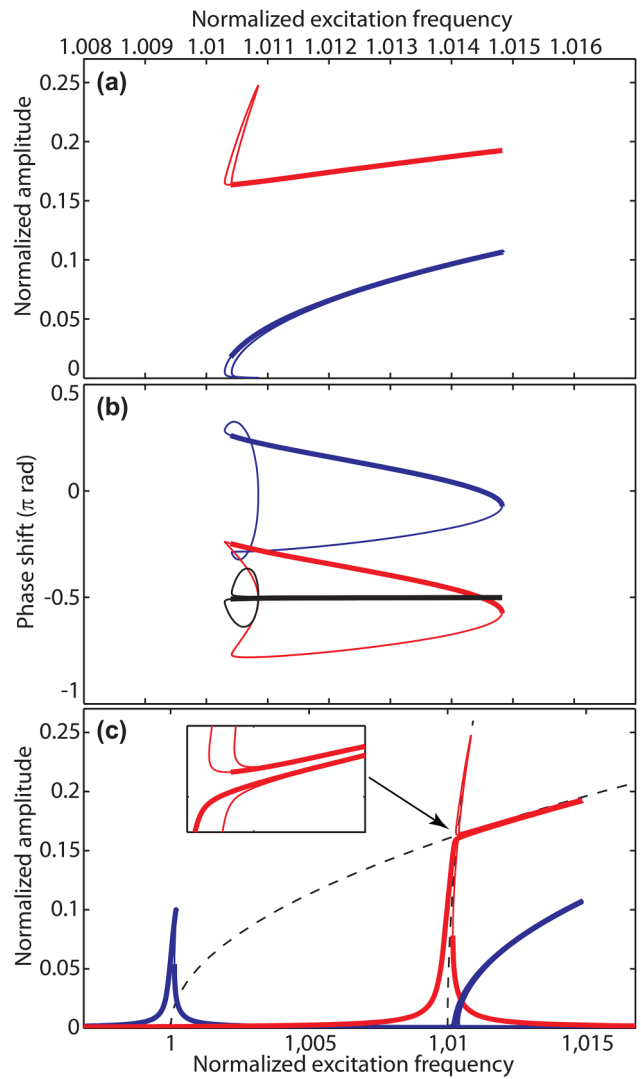


FIG. 5. Characterization of the new set of solutions appearing with the elliptical transition of which one branch is stable. (a) Amplitude and (b) phase diagrams of the new solutions. (c) Superposition of the different solutions of the equations. The inset is a zoom at the beginning of the transition.

staying above the other solution. We then have two stable elliptical solutions but rotating in opposite directions.

This phenomenon is analogous to the one observed in the case of the coupling of companion modes in circular plates^{14,29} or in a string.¹⁵ It can be explained by a pitchfork bifurcation point, for which a single stable branch (associated with the planar solution) becomes unstable and gives birth to two stable (nonplanar) solutions, with the same amplitude but with different phase differences $\pm\pi/2$. The two stable nonplanar solutions have opposite directions of motion. More precisely, because F_1 and F_2 are both chosen nonzero in the

simulations, the pitchfork bifurcation is in fact degenerate, so that the computed branches have a slightly different topology: the $+\pi/2$ branch is connected to the stable planar motion branch, and the $-\pi/2$ is isolated, with a saddle-node bifurcation in the vicinity.³⁰

To better understand the origin of the elliptical transition, we have plotted in Fig. 5(c) (black dashed lines) the evolution of $\omega_{x,\text{eff}}$ versus the amplitude R_y and the backbone curve of the unperturbed y polarization [Eqs. (11) and (12)]. We see that the transition occurs when the two effective frequencies are crossing each other. We know that two linear resonators, linearly and symmetrically coupled, lead to anti-crossing phenomena. In our case, the nonlinearly coupled equations lead to a more complex configuration with the apparition of new solutions that correspond to the elliptical movement and the apparition of an isolated set of solutions. For the effective frequencies, the family of the second solution is characterized by the fact that the $\omega_{x,\text{eff}}$ can be higher than the y polarization (see Fig. 2 of the supplementary material).

Now, we examine the effects of nonlinear coupling on the higher modes. In this case, the nonlinearities actually strengthen and the hard spring behavior, characteristic of the fundamental mode shape, becomes soft spring. Moreover, for the second mode shape, we have $2\alpha = 13.82$ and $\alpha - 2\beta = -65.4528$ so that one polarization, depending on the relative phase φ , can increase or decrease the effective frequency of the other polarization. We do not pretend that our analysis exhausts all the possibilities of these nonlinear couplings; however, the main characteristics observed for the fundamental mode also apply to the second mode. Figure 6 presents MANLAB simulations performed on the second mechanical mode with a frequency difference between polarizations of 2%. Figure 6(a) presents the continuation amplitude diagram where we observe again the elliptical transition on the higher polarization. As the second polarization is excited, we observe first the planar oscillation that exhibits soft spring behavior and the curve is bent to the left. As the amplitude increases, we reach the transition and the elliptical regime can occur. As the backbone curve of the elliptical movement is always oriented to the right (it depends only on α which is positive and then behave as hard spring), it results in a direction change in the amplitude continuation diagram. These elliptical solutions have been experimentally reported in Ref. 20. Figure 6(b) presents the closed family of solutions that consists once again in part of the truncated part of the y polarization that is unstable and of other elliptical solutions. The transition occurs for lower amplitudes as the term $-\alpha + 2\beta = 65.48$ for the second mode shape compared to 1.48 for the first mode shape. The backbone curves for the elliptical regime [Eqs. (14) and (15)] are presented in (a) and are once again in good agreement with simulations.

The case of higher modes is extremely similar to the second mode with a transition appearing for still smaller amplitudes. As well, for higher modes, the α terms become negligible compared to the β terms and the backbone curves [Eqs. (14) and (15)] for the elliptical regime tend to the equation $\omega_{y/x,e} = 1 + \frac{\mu}{2} + \frac{\alpha}{2} R_{y/x}^2$. We did not seek numerically the

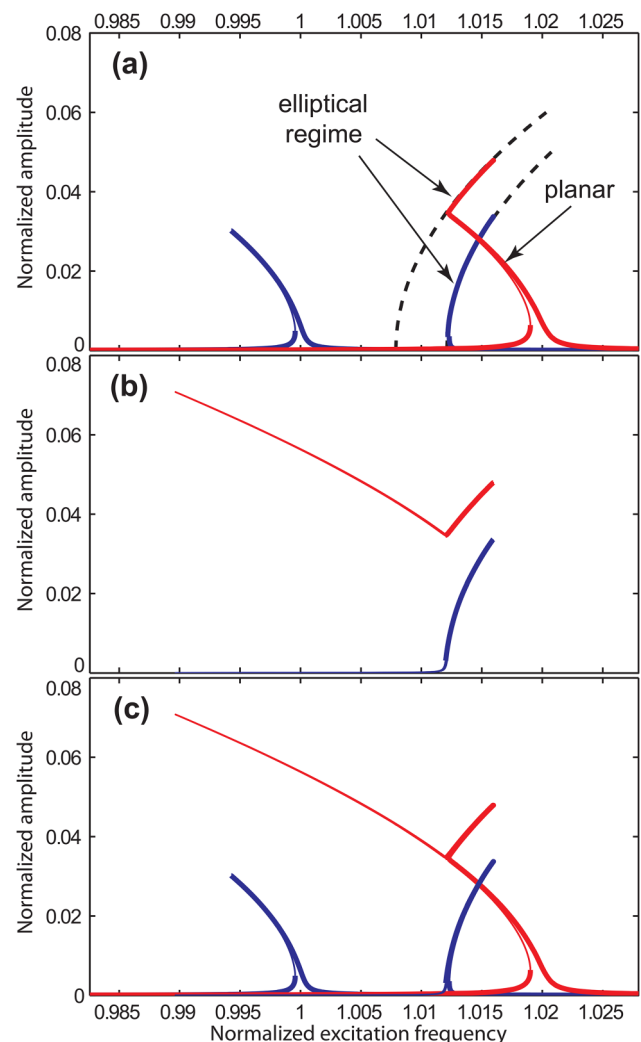


FIG. 6. Characterization of the elliptical transition for the second mode. (a) Frequency response of the polarizations showing soft spring Duffing behavior. Once again, for the higher polarization, the elliptical regime is observed with hard spring behavior. The dashed lines present the analytical backbone curves for the elliptical regime [Eqs. (14) and (15)]. (b) New isolated set of solutions corresponding to the elliptical regime. (c) Superposition of the two sets of solutions.

existence of the isolated solutions for mode 3 or higher, but we see no reasons why they would disappear.

V. DISCUSSION

Several more aspects of the elliptical transition are worth discussing.

Firstly, the analytical treatment was based on the fact that the phase difference, φ , increases through the first resonance and then begins to decrease in the second until it locks at $\pi/2$ during the elliptical regime [see Fig. 2(d)], i.e., the model

is based on two well separated polarizations. As a consequence, our model is not well suited for very low quality factors or polarizations very close in frequency. The equation that roughly characterizes the frontier of our model has been given above: $\mu > 2/Q$. This means, for example, that for $\mu = 0.01$, we must have $Q > 200$, that is, our case experimentally. To examine the effects of lower Q values, we present in Fig. 7 a series of simulations with quality factors of 10^4 , 2000, 500, 200, 100, 50, and 20, the same for the two polarizations, the excitation being increased accordingly to keep the same amplitudes ($QF = \text{constant}$). The value of $Q = 10\,000$ corresponds to the parameters used in Fig. 3 ($\mu = 0.01$) which serves here as a reference. For $Q = 2000$, the peaks enlarge as expected, but no significant change is observed. For $Q = 500$, the two resonances begin to merge, but the phase locking at $\pi/2$ is still clearly visible. We note an earlier emergence of the transition since the amplitude increases for lower frequencies. At $Q = 200$, the peaks merge even more and the phase locking is not so well pronounced. For $Q = 100$, the phase difference never reaches $\pi/2$, and, finally, for very low Q , only one very large peak is observable hiding the two polarizations. Note that for the lowest values of Q , when the two resonance curves merge, if the system is excited at a frequency in the overlap, the observed oscillations would also be elliptical with a major axis of the ellipse that would depend on the relative phase between polarizations. However, in this case, these ellipses are really trivial and would be observed even without nonlinear coupling terms. These ellipses, obtained for merged resonance curves, have to be clearly differentiated from the elliptical transition observed when the two resonances are well separated.

Secondly, once the elliptical regime is reached, the fundamental mode can be observed for a wide frequency range compared to its linear width. It is interesting to predict the end of this elliptical resonance. This aspect is not trivial in the general case but can be reasonably treated in some favorable cases. In the following, such a case is examined that corresponds to Fig. 3 ($\mu = 1\%$). Just considering the energy balance, there are two sources of dissipation and two sources of energy injection that depend on the relative phase of the motions with the excitation, the phase difference being locked during the elliptical regime. On the one hand, the dissipated power is given by $R_x^2/2Q + R_y^2/2Q$ (we neglect higher harmonic contributions). Remembering that during this regime one has $R_x^2 \simeq R_y^2 - R_{y,c}^2$, the dissipated power can be written as $(2R_y^2 - R_{y,c}^2)/2Q$. On the other hand, the injected power can be written as $F_1 R_x \sin(-\theta)/2 + F_2 R_y \sin(-\theta - \varphi)/2$. In our example, $QF_1 = 0.1$ and $QF_2 = 0.25$ so that $F_2 > F_1$, and for the jump, we have $\theta + \varphi \simeq -\pi/2$ leading to $\theta \simeq -\pi$. So, the injected power can be simplified as $F_2 R_y/2$ and now the energy balance corresponding to the jump is given by $QF_2 R_y = 2R_y^2 - R_{y,c}^2$. For the fundamental mode shape and a frequency difference of 1%, one has $R_{y,c} = 0.164$. As no term is negligible, the second order equation has to be solved to obtain the value of the maximum amplitude obtainable, $R_{y,max}$. Re-injecting this value into Eq. (14) gives the frequency at which the jump occurs. In our case, the calculations give a frequency for the jump of 1.01490 and the

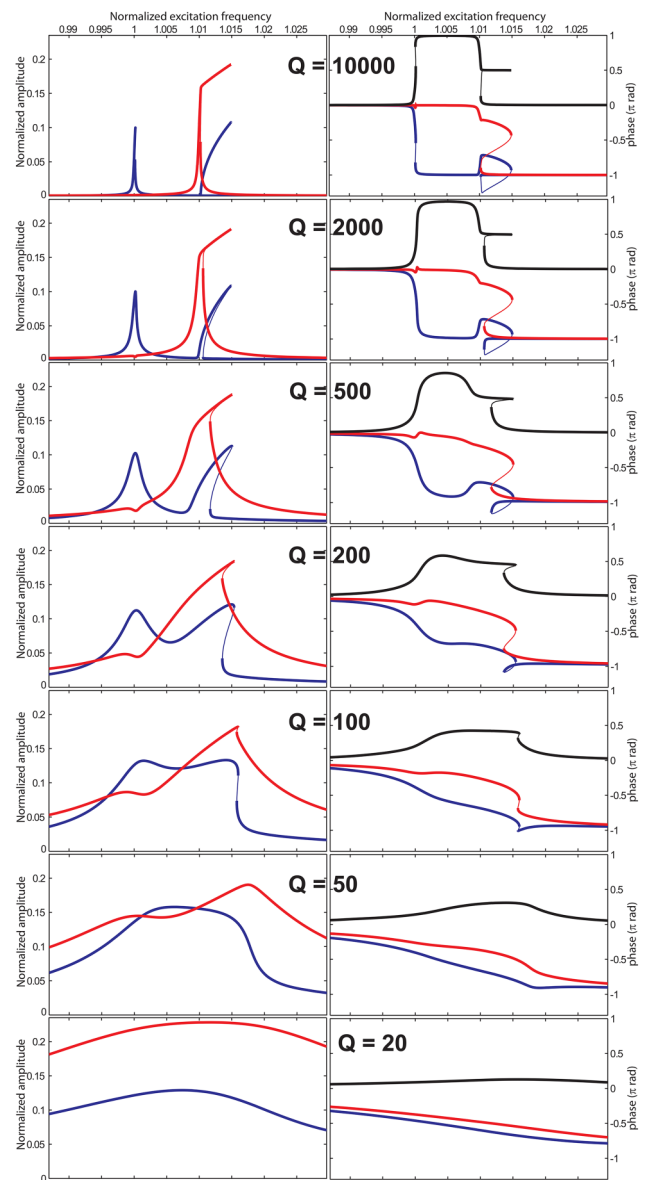


FIG. 7. Evolution of the elliptical transition as the quality factor decreases. The frequency difference is set to 1% and the excitation is increased to have $QF = \text{constant}$.

simulation a value of 1.01486, evidently in good agreement. However, this good quantitative agreement relies on the fact that the chosen parameters matched well with the hypothesis done for our analysis. In the general case, such an oversimplified analysis would not give such a precise estimation.

Thirdly, the nonlinear behaviors of our systems are governed by the combination of the terms α and β that correspond to nonlinear contributions coming from both potential

and kinetic energy. They combine in various and mode-dependent ways and can even have opposing effects. An illustration of the latter is the classical Duffing behavior which is described by the $(3\alpha - 2\beta)$ terms in Eq. (3). This explains why a hard spring Duffing behavior for the fundamental mode shape and soft spring for the higher modes shape are observed. Consequently, it would be interesting to modify α and β to change the response of our resonators. This approach has already been proposed and tested in NEMS by Refs. 31 and 32, for example, to improve the dynamic range of nanoresonators, but here we are also interested in how these modifications can alter the elliptical regime. Modifying the nonlinear coefficients can be realized for singly clamped nanowires over a limited range by applying a longitudinal tension, as can be done by applying a voltage difference between the nanowire and its environment. This creates a strong electric field at the apex that in turn results in a longitudinal electrostatic force. The rigidity of nanowires is small, and thus, this electrostatic tension term can be of the same order or even higher allowing to electrostatically tune the resonance frequencies of NNs over a wide range.³³ The contribution of the longitudinal electrostatic force to the potential energy is twofold. First, it changes the evolution of the stored energy as the amplitude increases and secondly, it modifies the linear shape of the mode. The consequence is that the value of α is now a function of the applied voltage V . For kinetic energy, the mode shape evolution also results in a variation of β . It is convenient here to define V_c as the voltage for which the generated longitudinal force is $T = \frac{EI}{L^2}$.²⁶ The mechanical effects of an applied voltage V then only depend on the ratio V/V_c . In Fig. 8, we present the evolution of α , β , $3\alpha - 2\beta$, and $-\alpha + 2\beta$ as a function of the applied voltage for the fundamental mode. Interestingly, the $3\alpha - 2\beta$ term that is positive for low voltages (hard spring behavior) cancels for intermediate voltages and becomes negative (soft spring behavior) for higher voltages. It means first that it is possible to cancel the cubic nonlinear terms and to obtain a linear response over a large amplitude range and secondly that soft spring behavior should be observable for highly strained nanowires. In fact, for very thin nanotubes (single or double wall nanotubes), we effectively only observe soft spring behavior during field emission experiments.³⁴ Concerning the elliptical transition, it remains over the whole voltage range and even appears for lower critical amplitudes as can be seen by the increasing value of $-\alpha + 2\beta$. Consequently, adding a longitudinal tension to the nanowire can modify the nonlinear response but does not remove the elliptical regime.

Finally, the analysis above shows the existence of an isolated set of solutions that in particular contains stable solutions, a fact explained by a degenerate pitchfork bifurcation, analogous to string vibrations.¹⁵ Figure 5(c) shows that there can be as many as seven solutions for some frequencies in which three are stable. Note that the third stable solution is in an isolated set and this means that practically this solution cannot be obtained by increasing quasi-statically the excitation frequency. Furthermore, the fact that these two elliptical solutions are very close in amplitude is insidious. In the four dimensional

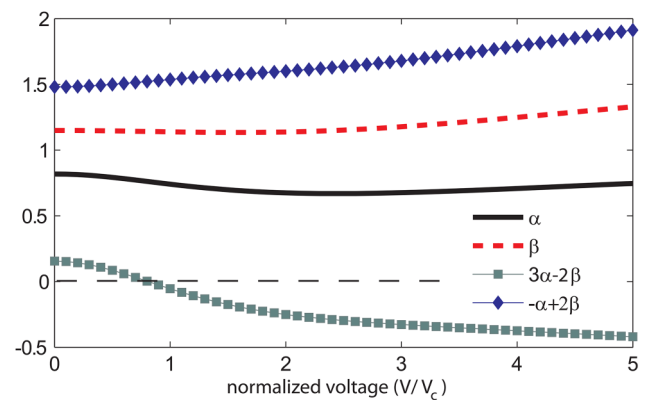


FIG. 8. Evolution of the parameters α , β , $3\alpha - 2\beta$, and $-\alpha + 2\beta$ for the fundamental mode as a function of the longitudinal tension in the simply clamped configuration.

state space that characterizes the system (we can choose R_x , R_y , θ , and φ as axes), these two stable solutions are very well separated since their projections on the φ axis are, respectively, $+\frac{\pi}{2}$ and $-\frac{\pi}{2}$. Thus, to obtain this solution, we have to perturb the system enough so as to reach the correct basin of attraction. This can be done *a priori* by adding temporarily another excitation such as a voltage pulse. In a macro circular plate, the isolated $-\pi/2$ solution was experimentally observed after a small mallet hit on the plate, enabling a jump from the $\pi/2$ solution to the $-\pi/2$ solution.¹⁴ A more interesting and sophisticated strategy to produce this state is to reach its basin of attraction by a controlled and reproducible procedure. Kozinsky *et al.*,³⁵ for example, have experimentally characterized the basin of attraction of a Duffing oscillator. By controlling the amplitude and delay of a preliminary excitation, they controlled their starting point in the phase space and could measure which final solution they obtained. Once characterized, they can obtain the desired solution at will. Another example of such a control is provided by the electromechanical parametron developed by the NTT laboratory.³⁶ In their system, the mechanical resonator is actuated by a piezoelectric modulation at twice its natural frequency. The resulting parametric resonance is bi-stable and two solutions can be obtained different in phase (0 or π). The oscillation can then be made to represent a binary digit by the choice between two stationary phases π radians apart. Our system presents several similarities with the parametron as we also have two elliptical solutions that can be very close in amplitude but whose phase difference is separated by π radians. Interestingly, Mahboob and Yamaguchi³⁶ have shown that they can prepare their system to obtain the desired solution with a yield that can reach 100%. Obtaining one or the other stable elliptical solution should then be possible by a precise preparation of the system.

The rather detailed analysis above is developed for the elliptical regime we observed for singly clamped resonators. Actually, the doubly clamped configuration has been much more investigated than the singly clamped and previous works

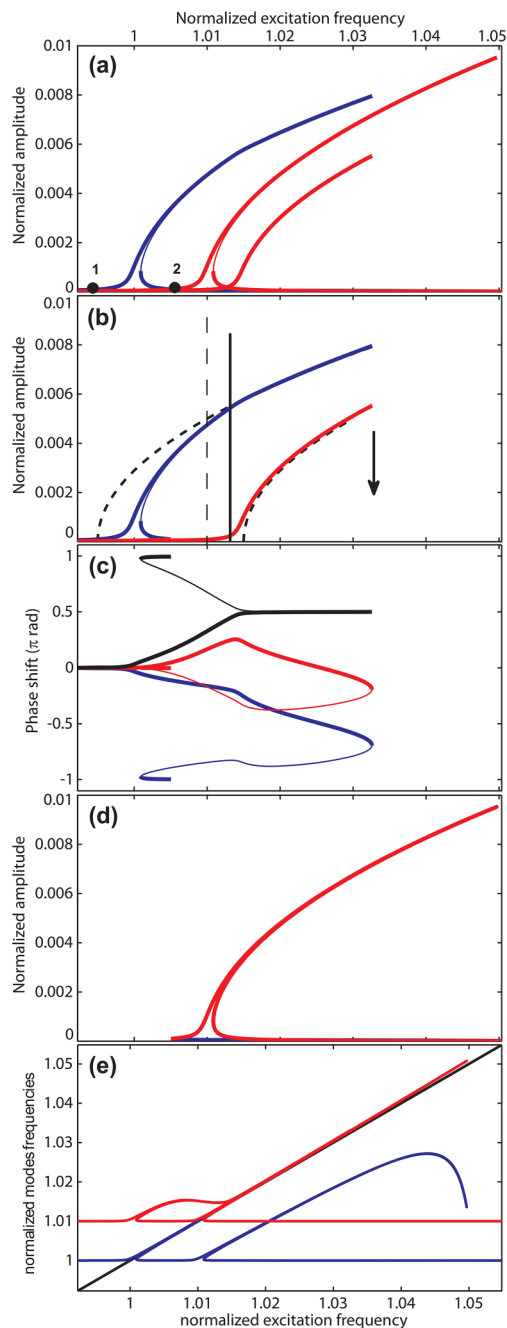


FIG. 9. Simulation of the elliptical transition in a doubly clamped configuration. (a) Total continuation diagram showing the emergence of the elliptical regime on the first polarization. (b) Part of the continuation diagram that would correspond to a frequency scan starting at point 1. (c) Phase diagram associated with the amplitude diagram presented in (b). (d) Second part of the continuation diagram. It would rather correspond to a frequency scan starting at point 2. Only the hard-spring planar Duffing behavior is observed on this polarization. (e) Evolution of the effective frequencies of the polarizations as a function of the excitation frequency.

present the apparition of an elliptical regime.^{16,17} It is therefore interesting to compare the two cases and to treat them with the same approach. As previously, we are not interested here in the case where the two resonance curves are merged and for which ellipses are trivial. For example, the article of Conley *et al.*³⁷ describing nonplanar dynamics of suspended nanotubes belongs to this category. Detailed models of nonlinearly coupled doubly clamped resonators can be found elsewhere.³⁷ For comparison, we simulate here a doubly clamped resonator with no applied stress and having a ratio $L/r = 100$. The oscillation amplitudes are normalized by the resonator's length.

It is well known that for a doubly clamped configuration, the nonlinear coupling is realized by the stretching of the resonator during oscillation. Physically, it means that we have cubic nonlinear terms in the potential energy but none in the kinetic energy. Consequently, the nonlinear equations describing the doubly clamped configuration are exactly the same as those in Eqs. (1) and (2) with $\beta = 0$ and α having a high positive value. Applying the same treatment as earlier one obtains Eqs. (3) and (4) but conserving only the α term. One now observes that the self tuning effect (3α) becomes more important than the effect of the other polarization [the term $2\alpha + \alpha \cos(2\varphi)$ vary between α and 3α and is equal to α for $\varphi = \pi/2$]. It means that if we excite the second polarization, the effective frequency of the lower polarization cannot reach the higher frequency. The elliptical transition is then no longer possible for the second polarization. However, if we excite the lower polarization, the effective frequency of the lower polarization will increase more rapidly than the higher one. If the frequency difference between polarizations is not too large, the effective frequency of the lower polarization can catch up to the effective frequency of the higher polarization and an elliptical transition can appear. From this analysis, it can be concluded that an elliptical regime for the doubly clamped configuration should only be possible for the lower polarization. Figure 9(a) presents MANLAB simulations for a doubly clamped configuration with no applied stress and $\mu = 1\%$. As expected, an elliptical transition is observed on the lower polarization, but the modifications corresponding to this transition are less evident compared to the singly clamped configuration. To clarify this continuation diagram, parts of this diagram are presented separately in Figs. 9(b) and 9(d). These parts would correspond more likely to experimental results depending if one starts a frequency scan at points 1 or 2 indicated in (a).

The situation corresponding to the initial point 1 is presented in Figs. 9(b) and 9(c) for the amplitude and phase diagrams, respectively. As the frequency is increased, we naturally begin to excite the lower polarization and, firstly, a planar hard spring resonance is observed. Interestingly, as the excitation frequency reaches the value of the natural resonant frequency of the second polarization [dashed vertical line in Fig. 9(b)], its amplitude does not increase as one might expect. The reason is that the effective frequency of the second polarization has been increased by the lower polarization amplitude as can be seen in Fig. 9(e) where the effective resonance frequencies of polarizations are plotted during the frequency scan (the same principle as in Fig. 4). As the frequency and R_x still increase, the

elliptical transition limit is reached [schematically represented by the black vertical line in (b)]. As previously, the elliptical regime is characterized by a value of φ that locks on $\pi/2$, an abrupt change in the slope of $R_x(\omega)$, an increase of R_y , and the two effective frequencies being very close. As the frequency is still increased, the ellipse enlarges and, finally, the system jumps out of the resonance. In contrast, starting at point 2, for example, by turning on the generator at this frequency, the resonance curve presented in Fig. 9(d) is obtained. It corresponds to the excitation of the planar hard spring second polarization at the expected value. A high amplitude was used to verify that no transition is observed. In Fig. 9(e), it can be seen that, as expected, the effective frequency of the lower polarization is increased but cannot reach the driving frequency.

As previously, the backbone curves corresponding to the elliptical regime can be estimated. This time, the critical amplitude, $R_{x,c}$, for which the transition occurs, is given by $R_{x,c} = \sqrt{\frac{3\mu}{\alpha}}$ and during the elliptical regime, $R_x^2 \simeq R_y^2 + R_{x,c}^2$. This leads to the backbone curves $\omega_{x,e} = 1 - \frac{\mu}{2} + \frac{\alpha}{2} R_x^2$ and $\omega_{y,e} = 1 + \frac{3\mu}{2} + \frac{\alpha}{2} R_y^2$. These backbone curves are plotted in Fig. 9(b), showing a good agreement with the simulations.

Finally, in the simulation presented here, no mechanical tension was applied to the nanowire. The application of a mechanical stress only changes the value of α , and, consequently, it does not change the principle of the elliptical transition. As well, the modeling of the higher modes results in an increase of the α values, but the elliptical regime remains.

VI. CONCLUSION

The intriguing elliptical regime comes about naturally from standard coupling intrinsic to a large class of nanometric resonators with two degrees of freedom. In this work, we attempt to give a full but comprehensible treatment useful for active researchers in the field of NEMS with an attention to providing simple guidelines to understand measurements and interesting new mechanical responses to explore. Specifically, the article contains analytical expressions characterizing the emergence of the transition as a function of the frequency difference between the polarizations and the evolution of the obtained ellipses that were given. We also showed the existence of a new set of solutions for which one branch is stable and could have potential applications. The comparison of nonlinearities between the singly and doubly clamped configurations showed that an elliptical transition appears in both configurations but on different polarizations. The better understanding of this transition can open original perspectives for NEMS applications.

SUPPLEMENTARY MATERIAL

The supplementary material includes a schematic of the experimental SEM configuration used for the observations of the elliptical transition, a detailed treatment of the 2D nonlinear equations of coupled polarizations leading to the emergence of the elliptical transition, and the two-time scale treatment of these equations.

ACKNOWLEDGMENTS

This research has been carried out within the “Plateforme Nanotube et Nanofil de Lyon.” This work is supported by the French Research Agency (ANR) through the projects (Nos. NEMSPIEZO ANR-08-NANO-015 and FOCUS-13-BS10-0012). The authors thank O. Arcizet for fruitful discussions.

REFERENCES

- H. W. Ch. Postma, I. Kozinsky, A. Husain, and M. L. Roukes, *Appl. Phys. Lett.* **86**, 223105 (2005).
- M. H. Matheny, L. G. Villanueva, R. B. Karabalin, J. E. Sader, and M. L. Roukes, *Nano Lett.* **13**, 1622 (2013).
- R. B. Karabalin, M. C. Cross, and M. L. Roukes, *Phys. Rev. B* **79**, 165309 (2009).
- H. J. R. Westra, M. Poot, H. S. J. van der Zant, and W. J. Venstra, *Phys. Rev. Lett.* **105**, 117205 (2010).
- A. Eichler, M. del Alamo Ruiz, J. A. Plaza, and A. Bachtold, *Phys. Rev. Lett.* **109**, 025503 (2012).
- A. H. Nayfeh, *Nonlinear Interactions* (John Wiley & Sons, 2000).
- R. Kuether, L. Renson, T. Detroux, C. Grappasonni, G. Kerschen, and M. S. Allen, *J. Sound Vib.* **351**, 299 (2016).
- M. Monteil, O. Thomas, and C. Touzé, *Appl. Acoust.* **89**, 1 (2015).
- M. Jossic, B. Chomette, V. Denis, O. Thomas, A. Mamou-Mani, and D. Roze, *J. Acoust. Soc. Am.* **144**, 431 (2018).
- C. Chen, D. H. Zanette, D. A. Czaplewski, S. Shaw, and D. López, *Nat. Comm.* **8**, 15523 (2017).
- A. Z. Hajjaj, M. A. Hafiz, and M. I. Younis, *Sci. Rep.* **7**, 41820 (2017).
- P. Taheri-Tehrani, A. Guerrieri, M. Defoort, A. Frangi, and D. A. Horsley, *Appl. Phys. Lett.* **111**, 183505 (2017).
- S. I. Chang, A. K. Bajaj, and C. M. Krousgrill, *Nonlinear Dyn.* **4**, 433 (1993).
- O. Thomas, C. Touzé, and A. Chaigne, *J. Sound Vib.* **265**, 1075 (2003).
- O. Thomas, A. Lazarus, and C. Touzé, in *Proceedings of the ASME 2010 International Design Engineering Technical Conferences & Computers and Information in Engineering Conference, IDETC/CIE 2010* (ASME Digital Collection, Montreal, 2010).
- C. H. Ho, R. A. Scott, and J. G. Easley, *Int. J. Non-Linear Mech.* **10**, 113 (1975).
- C. H. Ho, R. A. Scott, and J. G. Easley, *J. Sound Vib.* **47**, 333 (1976).
- F. Pai and A. H. Nayfeh, *Int. J. Non-Linear Mech.* **25**, 455 (1990).
- W. K. Lee, K. S. Lee, and C. H. Pak, *Nonlinear Dyn.* **52**, 217 (2008).
- S. Perisanu, T. Barois, A. Ayari, P. Poncharal, M. Choueib, S. T. Purcell, and P. Vincent, *Phys. Rev. B* **81**, 165440 (2010).
- R. Arquier, S. Karkar, A. Lazarus, O. Thomas, C. Vergez, and B. Cochelin, Manlab 2.0: An interactive path-following and bifurcation analysis software, Technical Report, Laboratoire de Mécanique et d'Acoustique, CNRS, see <http://manlab.lma.cnrs-mrs.fr>, 2005–2011.
- B. Cochelin and C. Vergez, *J. Sound Vib.* **324**, 243 (2009).
- A. Lazarus and O. Thomas, *C. R. Mécanique* **338**, 510 (2010).
- B. Bentvelsen and A. Lazarus, *Nonlinear Dyn.* **91**, 1349 (2018).
- S. Perisanu, P. Vincent, A. Ayari, M. Choueib, D. Guillot, M. Bechelany, D. Cornu, P. Miele, and S. T. Purcell, *Phys. Status Solidi A* **204**, 1645 (2007).
- S. Perisanu, V. Gouttenoire, P. Vincent, A. Ayari, M. Choueib, M. Bechelany, D. Cornu, and S. T. Purcell, *Phys. Rev. B* **77**, 165434 (2008).
- Figures 2(a) and 2(b) have been obtained by solving the following two equations where the coupling terms between polarizations has been removed:

$$(1 + \beta x^2)\ddot{x} + \frac{1}{Q}\dot{x} + (1 + \alpha x^2 + \beta x^2)x = F_1 \cos(\Omega t),$$

$$(1 + \beta y^2)\ddot{y} + \frac{1}{Q}\dot{y} + (1 + 2\mu + \alpha y^2 + \beta y^2)y = F_2 \cos(\Omega t).$$
- A. I. Manevitch and L. I. Manevitch, *Meccanica* **38**, 335 (2003).

- ²⁹C. Touzé, O. Thomas, and A. Chaigne, *J. Sound Vib.* **258**, 649 (2002).
- ³⁰W. Lacarbonara, *Nonlinear Structural Mechanics* (Springer, 2013).
- ³¹N. Kacem, J. Arcamone, F. Perez-Murano, and S. Hentz, *J. Micromech. Microeng.* **20**, 045023 (2010).
- ³²L. G. Villanueva, R. B. Karabalin, M. H. Matheny, D. Chi, J. E. Sader, and M. L. Roukes, *Phys. Rev. B* **87**, 024304 (2013).
- ³³S. T. Purcell, P. Vincent, C. Journet, and V. T. Binh, *Phys. Rev. Lett.* **89**, 276103 (2002).
- ³⁴A. Descombin, P. Poncharal, A. Pascale-Hamri, M. Choueib, R. Diehl, P. Vincent, S. T. Purcell, and S. Perisanu “Giant, voltage tuned, Q-factors of single wall carbon nanotubes and graphene at room temperature” (to be published).
- ³⁵I. Kozinsky, H. W. Ch. Postma, O. Kogan, A. Husain, and M. L. Roukes, *Phys. Rev. Lett.* **99**, 207201 (2007).
- ³⁶I. Mahboob and H. Yamaguchi, *Nature Nanotech.* **3**, 275 (2008).
- ³⁷W. G. Conley, A. Raman, C. M. Krousgrill, and S. Mohammad, *Nano Lett.* **8**, 1590 (2008).